

Field Tuning Beyond the Heat Death of a Charge-Density-Wave Chain

Manuel Weber^{1, 2, *} and James K. Freericks¹

¹*Department of Physics, Georgetown University, Washington, DC 20057, USA*

²*Max-Planck-Institut für Physik komplexer Systeme, Nöthnitzer Str. 38, 01187 Dresden, Germany*

(Dated: July 12, 2021)

Time-dependent driving of quantum systems has emerged as a powerful tool to engineer exotic phases far from thermal equilibrium; when the drive is periodic this is called Floquet engineering. The presence of many-body interactions can lead to runaway heating, so that generic systems are believed to heat up until they reach a featureless infinite-temperature state. Finding mechanisms to slow down or even avoid this heat death is a major goal—one such mechanism is to drive toward an even distribution of electrons in momentum space. Here we show how such a mechanism avoids the heat death for a charge-density-wave chain in a strong dc electric field; minibands with nontrivial distribution functions develop as the current is prematurely driven to zero. We also show how the field strength tunes between positive, negative, or close-to-infinite effective temperatures for each miniband. These results suggest that nontrivial metastable distribution functions should be realized in the prethermal regime of quantum systems coupled to slow bosonic modes.

The possibility to induce exotic nonequilibrium states with time-dependent electromagnetic fields in solid-state systems or in optical lattices has boosted the interest in driven quantum matter [1]. A current focus has been on *Floquet* systems where a time-periodic drive can realize novel topological phases [2, 3] or time crystals [4–6]. Because time-dependent Hamiltonians break energy conservation, the presence of many-body interactions, like a coupling to a bath or to phonons, inevitably leads to incoherent scattering and thereby to unintentional heating effects [7, 8]. Under which circumstances the looming heat death can be delayed [9–13] or even avoided [14–16] in a driven many-particle system, is an ongoing research topic that is of immediate importance for the experimental realization of novel out-of-equilibrium phases [17, 18]. For instance, the breakdown of ergodicity in the many-body-localized phase [19] has been considered as a microscopic process to avoid the heat death [14–16].

Given a periodically-driven system that does not heat up indefinitely, we study the logical follow-up questions: What does the steady state look like and how is it reached as a function of time? To this end, we consider a minimal interacting model where itinerant electrons on a chain are coupled to adiabatic phonons. Starting from a thermal state, we drive our system with a dc electric field, representing the simplest realization of a Floquet system (due to Bloch oscillations). This setup allows us to sample the initial states with a classical Monte Carlo method and reach the steady state on lattice sizes much larger than in state-of-the-art exact-diagonalization studies. To characterize our final states, we look at the frequency-resolved electron distribution function. In thermal equilibrium, the occupation of states is governed by the Fermi-Dirac distribution $f_{\text{eq}}(\omega) = 1/[\exp(\beta\omega) + 1]$ and only depends on the inverse temperature $\beta = 1/k_{\text{B}}T$. The fluctuation-dissipation theorem relates $f_{\text{eq}}(\omega)$ to the ratio of lesser and retarded single-particle Green's functions (defined below). In the same way, we define a nonequilibrium

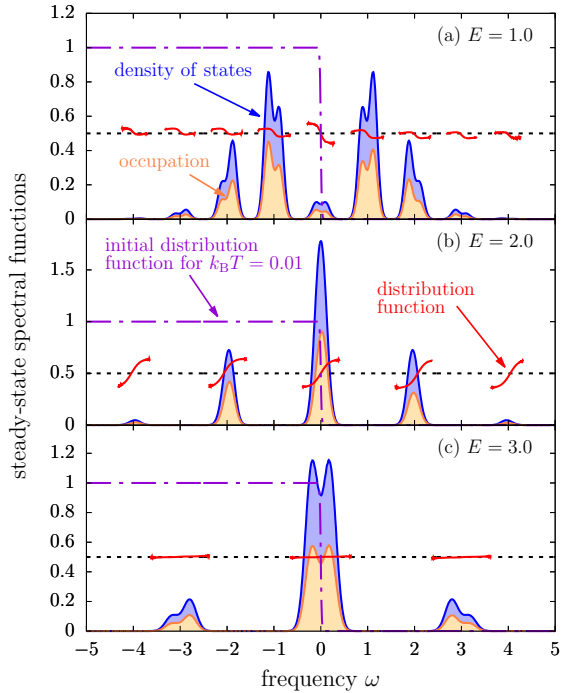


FIG. 1. Steady-state spectral functions. Density of states, occupation, and distribution function for different electric fields. Here, $k_{\text{B}}T = 0.01$, $L = 42$, $\lambda = 0.5$.

distribution function $f_{\infty}(\omega)$ for the steady state. Only if our system reaches a thermal state, will $f_{\infty}(\omega)$ correspond to $f_{\text{eq}}(\omega)$ with a renormalized temperature. Our main results are shown in Fig. 1. The steady-state spectral functions consist of minibands centered at integer multiples of the electric field (due to the Wannier-Stark ladder formation). For each miniband, we find Fermi-Dirac-like distribution functions with negative, positive, or zero slope corresponding to positive, negative, or infinite effective temperatures, respectively. The cases with nontrivial distribution functions are highly nonequilib-

rium, because the distribution function should be a single one for all minibands, not a different one for each miniband; the midpoints of each miniband also follow a separate distribution function. Furthermore, the proximity to the heat-death scenario can be tuned by adjusting the electric field. We explain below how this arises due to competing localization effects.

To study the nontrivial properties of the steady state, we consider the 1D Holstein model $\hat{H}(t) = \hat{H}_{\text{el}}(t) + \hat{H}_{\text{ph}}$ in an electric field. The electronic subsystem is given by

$$\hat{H}_{\text{el}}(t) = -J \sum_i (e^{-i\phi(t)} \hat{c}_i^\dagger \hat{c}_{i+1} + \text{H.c.}) + g \sum_i \hat{q}_i (\hat{n}_i - \frac{1}{2}). \quad (1)$$

The first term describes the nearest-neighbor hopping of spinless fermions with amplitude J where \hat{c}_i^\dagger (\hat{c}_i) creates (annihilates) an electron at site i . The time-dependent flux $\phi(t) = -E t \theta(t)$ incorporates a constant electric field E that is turned on at $t = 0$. We use the temporal gauge where $\hat{H}_{\text{el}}(t)$ becomes a Floquet system with periodicity $2\pi/E$ induced by the periodic bandstructure. In the second term, the local electron density $\hat{n}_i = \hat{c}_i^\dagger \hat{c}_i$ couples to the phonon displacement \hat{q}_i . The phonon Hamiltonian reads $\hat{H}_{\text{ph}} = \sum_i (\frac{K}{2} \hat{q}_i^2 + \frac{1}{2M} \hat{p}_i^2)$ with stiffness constant K , mass M , and momentum \hat{p}_i . We define the dimensionless coupling $\lambda = g^2/4KJ$, set $e = \hbar = c = 1$, and fix $J = 1$ as the unit of energy. All results are for $L = 42$ sites with periodic boundary conditions.

To efficiently solve for the real-time dynamics of $\hat{H}(t)$, we consider the adiabatic limit $M \rightarrow \infty$ of zero phonon frequency where the phonons lose their dynamics. Then, the phonon displacements become classical variables $\vec{q} = \{q_1, \dots, q_L\}$ and their equilibrium distribution

$$W_{\text{eq}}[\vec{q}] = \frac{1}{Z} e^{-\beta H_{\text{ph}}[\vec{q}]} Z_{\text{el}}[\vec{q}] \quad (2)$$

can be sampled using a Monte Carlo method [20], in combination with a parallel-tempering scheme to improve the sampling at low and intermediate $k_{\text{B}}T$ [21] (for details see Ref. [22]). Any observable $\langle \hat{O}(t) \rangle = \int d\vec{q} W_{\text{eq}}[\vec{q}] \langle \langle \hat{O}(t) \rangle \rangle_{\vec{q}}$ of the interacting system reduces to a weighted average over noninteracting expectation values

$$\langle \langle \hat{O}(t) \rangle \rangle_{\vec{q}} = \frac{1}{Z_{\text{el}}[\vec{q}]} \text{Tr} \left\{ e^{-\beta(\hat{H}_{\text{el}}[\vec{q}] - \mu \hat{N})} \hat{O}_{\vec{q}}(t) \right\} \quad (3)$$

for a fixed \vec{q} . Here, $Z_{\text{el}} = \text{Tr} \exp[-\beta(\hat{H}_{\text{el}} - \mu \hat{N})]$ is the partition function of the electronic subsystem with chemical potential μ and total electron number \hat{N} . While the phonons remain static, the electronic subsystem evolves according to the Heisenberg equations of motion for $\hat{c}_i^\dagger(t) = \hat{U}^\dagger(t, t_0) \hat{c}_i^\dagger(t_0) \hat{U}(t, t_0)$. Because $\hat{H}_{\text{el}}(\vec{q}, t)$ is quadratic, we only have to evolve the single-particle states using a Trotter decomposition. For a constant field E , the time-evolution operator $\hat{U}(t, t_0)$ only needs to be

calculated within its period $\tau = 2\pi/E$. For our simulations, we use the Trotter step $\Delta t = 2\pi/3360 \approx 0.002$ and calculate the steady-state behavior at 1000τ .

We prepare our system in a thermal state with initial temperature $k_{\text{B}}T$ and fix $\lambda = 0.5$. The phonon distribution $W_{\text{eq}}[\vec{q}]$ is entirely determined by $k_{\text{B}}T$. At $k_{\text{B}}T = 0$, the mean-field solution $q_i = (-1)^i \Delta/g$ is exact and leads to a band insulator with a single-particle gap $\Delta \approx 0.3404$. Translational symmetry is spontaneously broken by the periodic lattice distortion which gives rise to CDW order. Many-body interactions are gradually incorporated with increasing $k_{\text{B}}T$, as electrons start to scatter elastically from thermally-generated phonon displacements. Already small fluctuations in the phonon fields lead to a disordered phase, but the single-particle gap is only fully filled in at $k_{\text{B}}T \approx 0.1$, where short-range CDW correlations disappear. At higher temperatures, $W_{\text{eq}}[\vec{q}]$ eventually becomes a Gaussian with a variance $\sigma^2 \propto k_{\text{B}}T$. For further details on the equilibrium solution, see Ref. [22].

For a noninteracting system with a single band only, the application of a dc electric field leads to Bloch oscillations with periodicity $2\pi/E$ in time-evolved observables like the electronic energy $E_{\text{el}}(t) = \langle \hat{H}_{\text{el}}(t) \rangle / L$ or the current $j(t) = -J \sum_i (i e^{-i\phi(t)} \hat{c}_i^\dagger(t) \hat{c}_{i+1}(t) + \text{H.c.}) / L$. For our clean two-band insulator at $k_{\text{B}}T = 0$, interband Zener tunneling will also populate the initially-unoccupied upper band. The combination of Zener tunneling and Bragg reflections lead to very irregular oscillations [23]. A true steady state with constant energy and zero current is only reached for nonzero temperatures, as we see from the transient behavior of $E_{\text{el}}(t)$ and $j(t)$ in Figs. 2(a) and 2(b), respectively. The damping of the average energy and current results from the destructive interference between oscillating solutions for different phonon configurations. The gauge-invariant momentum distribution function [24] $n(k, t) = \langle \hat{c}_{k+\phi(t)}^\dagger(t) \hat{c}_{k+\phi(t)}(t) \rangle$ in Fig. 2(c) shows how the current vanishes before the system can reach an infinite-temperature state. The momentum distribution becomes a nontrivial even function of k in the long-time limit. This points towards a restoration of time-reversal symmetry in the steady state as the current is simultaneously quenched. A comparison of E_{el} between initial and final states in Fig. 2(d) reveals that heating effects are strongest at low $k_{\text{B}}T$ where the steady state gets close to the infinite-temperature result $E_{\text{el}} = 0$. Surprisingly, a higher initial temperature reduces the final energy and thereby the effective temperature of the steady state; this is similar to the inverse Mpemba effect [25]. In addition, the steady-state occupation $n(k)$ in Fig. 2(e) is close to a uniform distribution at low $k_{\text{B}}T$ and reaches its strongest k dependence around $k_{\text{B}}T = 1$. It appears that the proximity to coherent bands at low $k_{\text{B}}T$ allows for stronger heating, whereas localization effects due to phonon-induced disorder steadily reduce the system's ability to absorb energy with increasing $k_{\text{B}}T$.

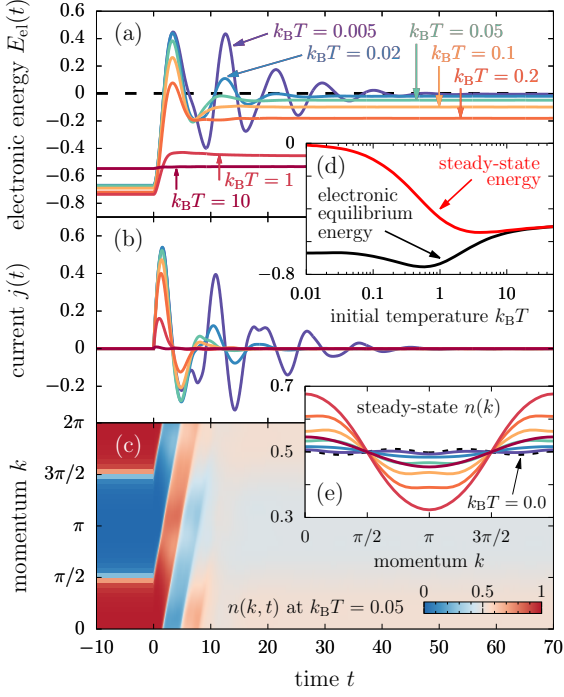


FIG. 2. Transient nonequilibrium dynamics: (a) Electronic energy and (b) current as a function of time for different initial temperatures. The dashed line in (a) represents the time average of $E_{\text{el}}(t)$ at $k_BT = 0$. (c) Gauge-invariant momentum distribution function at $k_BT = 0.05$. (d) Comparison of the equilibrium and steady-state electronic energies as a function of temperature. (e) Steady-state momentum distribution function for different temperatures. The labels in (a) also apply to (b) and (e). Here, $E = 1.0$, $L = 42$, $\lambda = 0.5$.

Note that E_{el} does not reach zero for $k_BT \rightarrow \infty$, neither in equilibrium nor for the steady state, because the variance of the phonon distribution scales as k_BT for large temperatures.

The spectral properties of the steady state can be inferred from the retarded and lesser Green's functions

$$G_{ij}^{\text{ret}}(t, t') = -i\Theta(t - t') \langle \{ \hat{c}_i(t), \hat{c}_j^\dagger(t') \} \rangle, \quad (4)$$

$$G_{ij}^<(t, t') = i \langle \hat{c}_j^\dagger(t') \hat{c}_i(t) \rangle. \quad (5)$$

Using the Wigner coordinates $t_{\text{ave}} = (t + t')/2$ and $t_{\text{rel}} = t - t'$, we define the Fourier transform $G_{\text{loc}}^\alpha(t_{\text{ave}}, \omega) = \int dt_{\text{rel}} e^{i(\omega + i\eta)t_{\text{rel}}} \sum_i G_{ii}^\alpha(t_{\text{ave}} + t_{\text{rel}}/2, t_{\text{ave}} - t_{\text{rel}}/2)/L$ of the local Green's functions. Then, the density of states becomes $A(t_{\text{ave}}, \omega) = -\text{Im} G_{\text{loc}}^{\text{ret}}(t_{\text{ave}}, \omega)/\pi$ and the occupation $A^<(t_{\text{ave}}, \omega) = \text{Im} G_{\text{loc}}^<(t_{\text{ave}}, \omega)/2\pi$. The steady-state spectra are shown in Fig. 1 for $k_BT = 0.01$. Their ratio defines the nonequilibrium distribution function,

$$f_\infty(\omega) = \frac{A^<(t_{\text{ave}} \rightarrow \infty, \omega)}{A(t_{\text{ave}} \rightarrow \infty, \omega)}, \quad (6)$$

which can be interpreted as a generalized nonequilibrium fluctuation-dissipation theorem in the long-time limit.

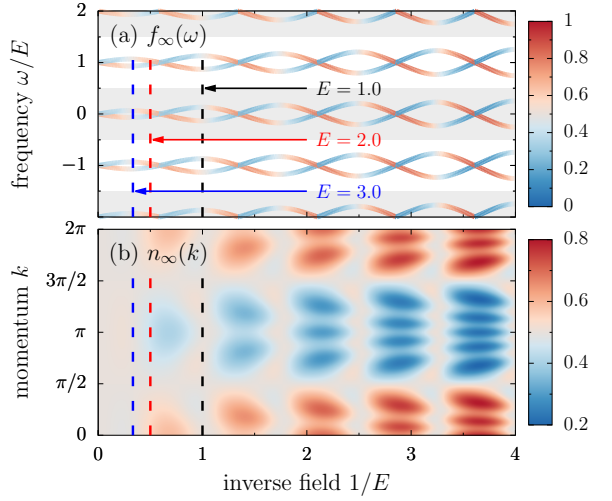


FIG. 3. Steady-state distribution functions for zero initial temperature. (a) The two quasienergies per Floquet energy window show (anti-) crossings as a function of inverse field. The color coding corresponds to the spectral distribution function $f_\infty(\omega)$. (b) The momentum distribution function $n_\infty(k)$ becomes flat when $f_\infty(\epsilon_\nu) = 1/2$. Dashed lines indicate the parameters chosen in Fig. 1 and Fig. 4. Here $\lambda = 0.5$.

We can understand the main spectral features in Fig. 1 from the zero-temperature limit. Due to the doubling of the unit cell by the Peierls distortion, the energy spectrum of the steady state in Fig. 3(a) consists of two interpenetrating Wannier-Stark ladders with a level spacing of E each. The color coding of the energy levels corresponds to $f_\infty(\omega)$, which we calculate using Floquet theory. Because the zero-temperature Green's functions do not decay with time, we average the spectra over t_{ave} —in this way, steady-state observables are defined consistently at $k_BT = 0$ and $k_BT > 0$. We obtain $f_\infty(\epsilon_\nu + mE) = \frac{2}{L} \sum_p \langle \hat{n}_{p\nu}(t = 0) \rangle$ for $\epsilon_{1,2} \in [-E/2, E/2]$, independent of $m \in \mathbb{Z}$. Here, $\hat{n}_{p\nu}(t = 0)$ is the number operator in the Floquet basis with momentum $p \in [0, \pi]$. Hence, $f_\infty(\omega)$ is given by the overlap of the Floquet states with the initially occupied states. Within each Floquet energy window in Fig. 3(a), we find intervals of E where the lower (upper) band has a higher f_∞ corresponding to an effective positive (negative) temperature per miniband in Fig. 1(a) [Fig. 1(b)]. The two regimes are separated by a level crossing in the zone center as well as an avoided level crossing at the zone boundary. Zener tunneling at the avoided crossings lifts the Wannier-Stark localization and leads to an equal occupation of the two levels corresponding to an effective infinite temperature in Fig. 1(c). At these resonances, the gauge-invariant momentum distribution function $n_\infty(k)$ is exactly $1/2$ for all k , as shown in Fig. 3(b) and proved in the Supplemental Material [26]. When $1/E$ is tuned off-resonance, $n_\infty(k)$ increasingly gains structure with each resonance that is crossed. Resonance-induced delocalization has been observed ex-

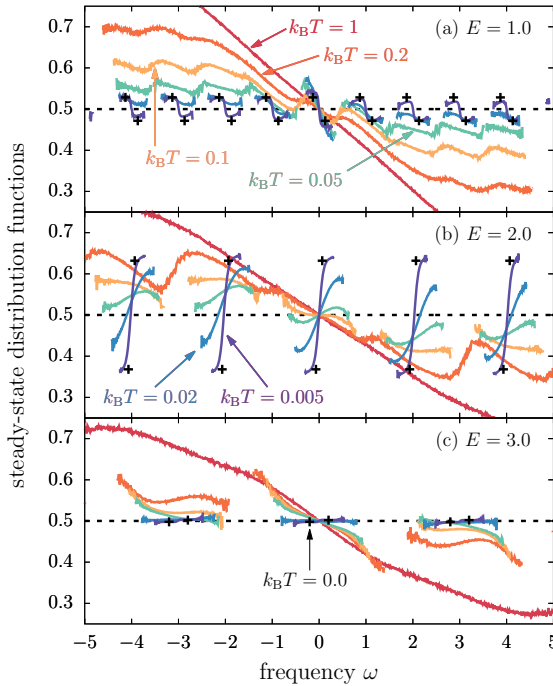


FIG. 4. Steady-state distribution functions for different initial temperatures. Here, $L = 42$ and $\lambda = 0.5$.

perimentally in semiconductor superlattices [27].

By introducing thermal fluctuations into the Floquet system via a nonzero initial $k_B T$, we can explain the spectral properties of Fig. 1. The phonon disorder lifts the $L/2$ -fold degeneracy of each Floquet level such that the delta peaks in the spectra get broadened. Then, we can obtain $f_\infty(\omega)$ on a continuous interval around the original levels as long as the spectral weight is not too small. We study the effect of the initial temperature on $f_\infty(\omega)$ in greater detail in Fig. 4. While the distributions per miniband mainly get smeared out for positive effective temperatures in Fig. 4(a), increasing phonon fluctuations reverse the negative-temperature distributions as a function of $k_B T$ in Fig. 4(b). The flat distributions in Fig. 4(c) remain rather flat for a broad range of $k_B T$. Moreover, the phonon fluctuations lift the degeneracy of $f_\infty(\omega)$ between the different Floquet zones such that the focal points of each miniband follow an overall distribution function. As $k_B T$ increases, the latter slowly transforms into a Fermi-Dirac-like distribution with an effective temperature that decreases. Above $k_B T \approx 1.0$, $f_\infty(\omega)$ is close to the initial thermal distribution and its effective temperature increases again, as suggested by the steady-state energy in Fig. 2(d).

We can interpret the interplay between initial temperature and electric field in terms of competing localization mechanisms. At high temperatures, the strong Gaussian phonon disorder promotes Anderson localization. Then, the application of an electric field enhances the localiza-

tion length [28], which only leads to small heating when approaching the steady state. Hence, $f_\infty(\omega)$ becomes flatter with increasing E , as we see in Fig. 4 for $k_B T = 1$. Only if E is strong enough compared to the phonon disorder, do signatures of Wannier-Stark localization appear, as its localization length is proportional to $1/E$ [29]. Therefore, the steady-state features at $k_B T \ll 1$ are governed by the Floquet solution. While each Floquet zone is populated equally at $k_B T = 0$, the nontrivial overall distribution for $k_B T > 0$ seems to be a partial memory effect of $f_{\text{eq}}(\omega)$. We saw that heating effects are strongest at low $k_B T$, where the system becomes a coherent band insulator. Although observables at zero temperature never decay towards a true steady state, a time average over all $t > 0$ is consistent with the steady-state results at $k_B T \rightarrow 0$, as shown in Fig. 4 for $f_\infty(\omega)$, in Fig. 2(a) for E_{el} , or in Fig. 2(e) for $n_\infty(k)$ (for further data, see the Supplemental Material). The higher absorption of heat at low $k_B T$ is thus determined by an easier ability for the system to equally occupy all electronic states as time proceeds.

In conclusion, we demonstrated for a simple interacting model of itinerant electrons coupled to classical phonons that the application of a dc electric field—contrary to common belief—does not lead to a featureless infinite-temperature state (unless the system is tuned to a zero-temperature resonance). Instead, the heating of the electronic subsystem stops as the current is prematurely driven to zero due to the symmetrization of the momentum distribution function. We obtain strongly nonequilibrium steady states with Fermi-Dirac-like distribution functions for each Floquet miniband. The final distribution function is tuned by the strength of the electric field. We found that competing Wannier-Stark and Anderson localization effects as well as resonance-induced delocalization explain the diverse properties of the steady state as a function of E and $k_B T$.

It remains open how quantum lattice fluctuations further affect these findings. While numerical simulations for nonequilibrium quantum phonons are currently prohibited by the unbound bosonic Hilbert space, the study of spin ladders coupled to slow modes suggest that localization effects remain important for long transient times [30], even if they do not persist to the steady state. We expect that the nonequilibrium distribution functions found in this work will still occur for low phonon frequencies, at least in a long-lived transient regime; once the current is driven to zero via the symmetrized momentum distribution, it is unclear what would destroy this for later times. Moreover, a dc electric field can lead to many-body localization in equilibrium setups even in the absence of disorder [31, 32]. It will be interesting to study whether more complicated interacting models inevitably have a heat death or continue to create nontrivial steady states. Further generalizations that include some of the quantum effects of the bosons (even if only semi-

classically) and that extend into higher dimensions, can provide additional insight into this complex phenomena.

Acknowledgments. We acknowledge helpful discussions with A. Kemper and D. Luitz. This work was supported by the U.S. Department of Energy (DOE), Office of Science, Basic Energy Sciences (BES) under Award DE-FG02-08ER46542. The authors gratefully acknowledge the Gauss Centre for Supercomputing e.V. (www.gauss-centre.eu) for funding this project by providing computing time on the GCS Supercomputer SuperMUC-NG at Leibniz Supercomputing Centre (www.lrz.de) (project-id pr53ju).

* Corresponding author: mweber@pks.mpg.de

- [1] D. N. Basov, R. D. Averitt, and D. Hsieh, Towards properties on demand in quantum materials, *Nature Materials* **16**, 1077 (2017).
- [2] T. Oka and S. Kitamura, Floquet Engineering of Quantum Materials, *Annual Review of Condensed Matter Physics* **10**, 387 (2019).
- [3] M. S. Rudner and N. H. Lindner, Band structure engineering and non-equilibrium dynamics in Floquet topological insulators, *Nature Reviews Physics* **2**, 229 (2020).
- [4] V. Khemani, A. Lazarides, R. Moessner, and S. L. Sondhi, Phase structure of driven quantum systems, *Phys. Rev. Lett.* **116**, 250401 (2016).
- [5] K. Sacha and J. Zakrzewski, Time crystals: a review, *Reports on Progress in Physics* **81**, 016401 (2018).
- [6] V. Khemani, R. Moessner, and S. L. Sondhi, A Brief History of Time Crystals, [arXiv:1910.10745](https://arxiv.org/abs/1910.10745) (2019).
- [7] L. D’Alessio and M. Rigol, Long-time Behavior of Isolated Periodically Driven Interacting Lattice Systems, *Phys. Rev. X* **4**, 041048 (2014).
- [8] A. Lazarides, A. Das, and R. Moessner, Equilibrium states of generic quantum systems subject to periodic driving, *Phys. Rev. E* **90**, 012110 (2014).
- [9] D. A. Abanin, W. De Roeck, and F. Huveneers, Exponentially Slow Heating in Periodically Driven Many-Body Systems, *Phys. Rev. Lett.* **115**, 256803 (2015).
- [10] D. V. Else, B. Bauer, and C. Nayak, Prethermal Phases of Matter Protected by Time-Translation Symmetry, *Phys. Rev. X* **7**, 011026 (2017).
- [11] M. Bukov, M. Heyl, D. A. Huse, and A. Polkovnikov, Heating and many-body resonances in a periodically driven two-band system, *Phys. Rev. B* **93**, 155132 (2016).
- [12] D. Abanin, W. De Roeck, W. W. Ho, and F. Huveneers, A Rigorous Theory of Many-Body Prethermalization for Periodically Driven and Closed Quantum Systems, *Communications in Mathematical Physics* **354**, 809 (2017).
- [13] D. J. Luitz, R. Moessner, S. L. Sondhi, and V. Khemani, Prethermalization without Temperature, *Phys. Rev. X* **10**, 021046 (2020).
- [14] A. Lazarides, A. Das, and R. Moessner, Fate of Many-Body Localization Under Periodic Driving, *Phys. Rev. Lett.* **115**, 030402 (2015).
- [15] P. Ponte, Z. Papić, F. Huveneers, and D. A. Abanin, Many-Body Localization in Periodically Driven Systems, *Phys. Rev. Lett.* **114**, 140401 (2015).
- [16] D. A. Abanin, W. De Roeck, and F. Huveneers, Theory of many-body localization in periodically driven systems, *Annals of Physics* **372**, 1 (2016).
- [17] A. Rubio-Abadal, M. Ippoliti, S. Hollerith, D. Wei, J. Rui, S. L. Sondhi, V. Khemani, C. Gross, and I. Bloch, Floquet Prethermalization in a Bose-Hubbard System, *Phys. Rev. X* **10**, 021044 (2020).
- [18] P. Peng, C. Yin, X. Huang, C. Ramanathan, and P. Capellaro, Floquet prethermalization in dipolar spin chains, *Nature Physics* **17**, 444 (2021).
- [19] D. M. Basko, I. L. Aleiner, and B. L. Altshuler, Metal insulator transition in a weakly interacting many-electron system with localized single-particle states, *Annals of Physics* **321**, 1126 (2006).
- [20] K. Michielsen and H. De Raedt, Quantum molecular dynamics study of the Su-Schrieffer-Heeger model, *Z. Phys. B Condens. Mat.* **103**, 391 (1997).
- [21] K. Hukushima and K. Nemoto, Exchange Monte Carlo Method and Application to Spin Glass Simulations, *J. Phys. Soc. Japan* **65**, 1604 (1996).
- [22] M. Weber, F. F. Assaad, and M. Hohenadler, Thermodynamic and spectral properties of adiabatic Peierls chains, *Phys. Rev. B* **94**, 155150 (2016).
- [23] J. Rotvig, A.-P. Jauho, and H. Smith, Bloch Oscillations, Zener Tunneling, and Wannier-Stark Ladders in the Time Domain, *Phys. Rev. Lett.* **74**, 1831 (1995).
- [24] R. Bertoncini and A. P. Jauho, Gauge-invariant formulation of the intracollisional field effect including collisional broadening, *Phys. Rev. B* **44**, 3655 (1991).
- [25] Z. Lu and O. Raz, Nonequilibrium thermodynamics of the Markovian Mpemba effect and its inverse, *Proc. Nat. Acad. Sci. (USA)* **114**, 5083 (2017).
- [26] See Supplemental Material at [url1](https://arxiv.org/abs/2003.08252) for details on the zero-temperature solution, additional results, Refs. [33–36], and data files for the results presented in this Letter.
- [27] H. Schneider, H. T. Grahn, K. v. Klitzing, and K. Ploog, Resonance-induced delocalization of electrons in GaAs-AlAs superlattices, *Phys. Rev. Lett.* **65**, 2720 (1990).
- [28] V. N. Prigodin, One-dimensional disordered system in an electric field, *JETP* **52**, 1185 (1980).
- [29] E. Cota, J. V. José, and G. Monsiváis, Stark-ladder resonances in ordered and disordered electrified chains, *Phys. Rev. B* **35**, 8929 (1987).
- [30] N. Y. Yao, C. R. Laumann, J. I. Cirac, M. D. Lukin, and J. E. Moore, Quasi-Many-Body Localization in Translation-Invariant Systems, *Phys. Rev. Lett.* **117**, 240601 (2016).
- [31] M. Schulz, C. A. Hooley, R. Moessner, and F. Pollmann, Stark Many-Body Localization, *Phys. Rev. Lett.* **122**, 040606 (2019).
- [32] E. van Nieuwenburg, Y. Baum, and G. Refael, From Bloch oscillations to many-body localization in clean interacting systems, *Proc. Nat. Acad. Sci. (USA)* **116**, 9269 (2019).
- [33] M. S. Rudner and N. H. Lindner, The Floquet Engineer’s Handbook, [arXiv:2003.08252](https://arxiv.org/abs/2003.08252) (2020).
- [34] J. H. Shirley, Solution of the Schrödinger Equation with a Hamiltonian Periodic in Time, *Phys. Rev.* **138**, B979 (1965).
- [35] G. S. Uhrig, M. H. Kalthoff, and J. K. Freericks, Positivity of the Spectral Densities of Retarded Floquet Green Functions, *Phys. Rev. Lett.* **122**, 130604 (2019).
- [36] J. Leo and A. MacKinnon, Stark-Wannier states and Stark ladders in semiconductor superlattices, *Journal of Physics: Condensed Matter* **1**, 1449 (1989).

Supplemental Material for

Field Tuning Beyond the Heat Death of a Charge-Density-Wave Chain

Manuel Weber^{1,2} and James K. Freericks¹

¹*Department of Physics, Georgetown University, Washington, DC 20057, USA*

²*Max-Planck-Institut für Physik komplexer Systeme, Nöthnitzer Str. 38, 01187 Dresden, Germany*

(Dated: July 12, 2021)

I. FLOQUET THEORY FOR THE PERFECTLY-DIMERIZED CHAIN

At zero initial temperature, the Holstein model driven by a constant electric field can be solved efficiently using Floquet theory. Here, we want to give a brief introduction to Floquet theory and outline the relevant steps for our solution, before we present additional results in the subsequent section. Our presentation of the basics of Floquet theory follows Ref. [1].

A. Basics of Floquet theory

For a time-dependent Hamiltonian $\hat{H}(t+T) = \hat{H}(t)$ with periodicity T , the Schrödinger equation ($\hbar = 1$)

$$i \frac{d}{dt} |\Psi(t)\rangle = \hat{H}(t) |\Psi(t)\rangle \quad (1)$$

can be solved using Floquet theory. The eigenstates of the time-evolution operator after evolving by one time period, $\hat{U}(t_0+T, t_0)$, are the so-called *Floquet states*. According to Floquet's theorem, these states can be expanded in terms of time-periodic states $|\Phi_\nu(t)\rangle$ via

$$|\Psi_\nu(t)\rangle = e^{-i\epsilon_\nu t} |\Phi_\nu(t)\rangle, \quad |\Phi_\nu(t+T)\rangle = |\Phi_\nu(t)\rangle, \quad (2)$$

with ϵ_ν the Floquet quasienergies. Because $|\Phi_\nu(t)\rangle$ has periodicity T , we can expand these states in a Fourier series with frequency $\Omega = 2\pi/T$,

$$|\Phi_\nu(t)\rangle = \sum_{m=-\infty}^{\infty} e^{-im\Omega t} |\phi_\nu^{(m)}\rangle. \quad (3)$$

Here, $|\phi_\nu^{(m)}\rangle$ is the m -th Fourier coefficient of $|\Phi_\nu(t)\rangle$. If we plug Eq. (2) and Eq. (3) into Eq. (1) and expand the Hamiltonian as

$$\hat{H}(t) = \sum_{m=-\infty}^{\infty} e^{-im\Omega t} \hat{H}^{(m)}, \quad (4)$$

we obtain the eigenvalue equation

$$(\epsilon_\nu + m\Omega) |\phi_\nu^{(m)}\rangle = \sum_n \hat{H}^{(m-n)} |\phi_\nu^{(n)}\rangle. \quad (5)$$

To determine ϵ_ν and $|\phi_\nu^{(m)}\rangle$, we only need to diagonalize the infinite-dimensional matrix

$$\hat{H}_{mn}^F = \hat{H}^{(m-n)} - m\Omega \delta_{mn}. \quad (6)$$

For the numerical diagonalization of \hat{H}^F , we introduce a cutoff that is large enough so that results are converged. A complete set of states is found by restricting all quasienergies to lie in the range $-\Omega/2 \leq \epsilon_\nu < \Omega/2$. For further details see Ref. [1] or the original work [2].

B. Holstein model at zero temperature

At zero temperature and half-filling, the phonon displacements in the Holstein model are perfectly dimerized and described by the mean-field ansatz $q_i = (-1)^i \Delta/g$. Then, the Holstein model in a constant electric field E can be partially diagonalized and we obtain the time-dependent two-band Hamiltonian

$$\hat{H}(t) = \sum_p \sum_{\alpha\beta} \hat{c}_{p\alpha}^\dagger \mathcal{H}_{p,\alpha\beta}(t) \hat{c}_{p\beta}. \quad (7)$$

Here, $\hat{c}_{p\alpha} = \hat{c}_{p+(\alpha-1)\pi}$ annihilates an electron with reduced momentum $p = 2\pi n/L$, $n = \{0, \dots, L/2 - 1\}$, and orbital index $\alpha = \{1, 2\}$. The single-particle Hamiltonian is

$$\hat{\mathcal{H}}_p(t) = \begin{pmatrix} \epsilon(p+Et) & \Delta \\ \Delta & -\epsilon(p+Et) \end{pmatrix}. \quad (8)$$

where $\epsilon(p) = -2J \cos p$. Because $\hat{\mathcal{H}}_p(t)$ has periodicity $T = 2\pi/E$, we can expand it according to Eq. (4) with $\Omega = 2\pi/T = E$. The only nonzero elements are

$$\hat{\mathcal{H}}_p^{(0)} = \begin{pmatrix} 0 & \Delta \\ \Delta & 0 \end{pmatrix}, \quad \hat{\mathcal{H}}_p^{(\pm 1)} = \begin{pmatrix} -Je^{\mp ip} & 0 \\ 0 & Je^{\mp ip} \end{pmatrix}. \quad (9)$$

With this, the eigenvalue equation (5) can be solved for each momentum p . Note that we have an additional orbital index. The Fourier expansion of the Floquet states can be represented as

$$|\phi_{p\nu}^{(m)}\rangle = \sum_{\alpha} \langle p\alpha | \phi_{p\nu}^{(m)} \rangle |p\alpha\rangle, \quad (10)$$

where $|p\alpha\rangle$ represents the eigenbasis of the physical states created by the corresponding creation operators.

1. Symmetries of the Floquet Hamiltonian

For the 1D Holstein model in a constant field, we want to give a few symmetries of the infinite-dimensional (Floquet) Hamiltonian that simplify its solution:

(i) The *momentum translation symmetry*

$$\hat{S}_p^\dagger \hat{\mathcal{H}}_p^F \hat{S}_p = \hat{\mathcal{H}}_{p=0}^F, \quad \hat{S}_{p,mn} = e^{-i p m} \delta_{mn} \quad (11)$$

$$\Rightarrow \langle p\alpha | \phi_{p\nu}^{(m)} \rangle = e^{-i p m} \langle p=0, \alpha | \phi_{p=0, \nu}^{(m)} \rangle \quad (12)$$

relates all expectation values to the $p = 0$ case. In particular, the Floquet quasienergies become independent of p , i.e., $\epsilon_{p\nu} = \epsilon_\nu$.

(ii) The *orbital (sublattice interchange) symmetry*

$$\hat{S}_p^\dagger \hat{\mathcal{H}}_p^F \hat{S}_p = \hat{\mathcal{H}}_p^F, \quad \hat{S}_{p,mn} = e^{-i \pi m} \hat{\sigma}_x \delta_{mn} \quad (13)$$

$$\Rightarrow \langle p\alpha | \phi_{p\nu}^{(m)} \rangle = e^{-i \pi m} \langle p\bar{\alpha} | \phi_{p\nu}^{(m)} \rangle \quad (14)$$

relates opposite orbitals α and $\bar{\alpha}$. Here, $\hat{\sigma}_x$ is the usual Pauli matrix.

(iii) The *particle-hole symmetry*

$$\hat{S}_p^\dagger \hat{\mathcal{H}}_p \hat{S}_p = -\hat{\mathcal{H}}_p, \quad \hat{S}_{p,mn} = e^{-i \pi m} \hat{\sigma}_z \delta_{mn} \quad (15)$$

$$\Rightarrow \langle p\alpha | \phi_{p\nu}^{(m)} \rangle = e^{-i \pi m} \langle p\alpha | \phi_{p\bar{\nu}}^{(-m)} \rangle \quad (16)$$

relates $\epsilon_\nu + m\Omega \rightarrow -\epsilon_\nu - m\Omega$.

2. Equilibrium solution

We prepare the initial state of our system in the half-filled ground state of the equilibrium Hamiltonian with $E = 0$. Below, we need $\langle \hat{c}_{p\alpha}^\dagger \hat{c}_{p\beta} \rangle$, which can be obtained from diagonalizing the Hamiltonian for each p and filling the lower level. We obtain

$$\langle \hat{c}_{p2}^\dagger \hat{c}_{p2} \rangle = \frac{\Delta^2}{2[\Delta^2 + \epsilon(p)^2 - \epsilon(p)\sqrt{\Delta^2 + \epsilon(p)^2}]}, \quad (17)$$

$$\langle \hat{c}_{p1}^\dagger \hat{c}_{p2} \rangle = \frac{\Delta [\epsilon(p) - \sqrt{\Delta^2 + \epsilon(p)^2}]}{2[\Delta^2 + \epsilon(p)^2 - \epsilon(p)\sqrt{\Delta^2 + \epsilon(p)^2}]}, \quad (18)$$

as well as the relations

$$\langle \hat{c}_{p1}^\dagger \hat{c}_{p1} \rangle = 1 - \langle \hat{c}_{p2}^\dagger \hat{c}_{p2} \rangle, \quad \langle \hat{c}_{p2}^\dagger \hat{c}_{p1} \rangle = \langle \hat{c}_{p1}^\dagger \hat{c}_{p2} \rangle. \quad (19)$$

C. Time-evolution operator in the Floquet basis

To calculate real-time observables, we need access to the time-evolved creation and annihilation operators. Using the equation of motion, we can trace the time evolution of any quadratic Hamiltonian back to an initial time t_0 , i.e.,

$$\begin{aligned} \hat{c}_{p\alpha}(t) &= \hat{U}^\dagger(t, t_0) \hat{c}_{p\alpha}(t_0) \hat{U}(t, t_0) \\ &= \sum_{\alpha'} \mathcal{U}_{p,\alpha\alpha'}(t, t_0) \hat{c}_{p\alpha'}(t_0). \end{aligned} \quad (20)$$

The time-evolution operator of the single-particle Hamiltonian can be obtained as

$$\begin{aligned} \mathcal{U}_{p,\alpha\alpha'}(t, t_0) &= \langle p\alpha | \hat{\mathcal{U}}(t, t_0) | p\alpha' \rangle \\ &= \sum_{\nu} \langle p\alpha | \hat{\mathcal{U}}(t, t_0) | \Psi_{p\nu}(t_0) \rangle \langle \Psi_{p\nu}(t_0) | p\alpha' \rangle \\ &= \sum_{\nu} \langle p\alpha | \Psi_{p\nu}(t) \rangle \langle \Psi_{p\nu}(t_0) | p\alpha' \rangle \\ &= \sum_{\nu} e^{-i\epsilon_\nu(t-t_0)} \langle p\alpha | \Phi_{p\nu}(t) \rangle \langle \Phi_{p\nu}(t_0) | p\alpha' \rangle. \end{aligned} \quad (21)$$

In combination with the Fourier expansion of the Floquet states in Eq. (3), we obtain the full time dependence of any observable from the eigenvalue solution of Eq. (6). This is particularly useful if we want to calculate integrals over time, as it is the case for the steady-state spectral functions considered below.

To shorten the notation below, we define the fermionic annihilation operators in the Floquet basis as

$$\hat{c}_{p\nu}(t_0) = \sum_{\alpha} \langle \Phi_{p\nu}(t_0) | p\alpha \rangle \hat{c}_{p\alpha}(t_0). \quad (22)$$

D. Spectral functions

Starting from the retarded and lesser Green's functions

$$G_{p,\alpha\beta}^{\text{ret}}(t, t') = -i\Theta(t - t') \left\langle \left\{ \hat{c}_{p\alpha}(t), \hat{c}_{p\beta}^\dagger(t') \right\} \right\rangle, \quad (23)$$

$$G_{p,\alpha\beta}^<(t, t') = i \left\langle \hat{c}_{p\beta}^\dagger(t') \hat{c}_{p\alpha}(t) \right\rangle, \quad (24)$$

we can determine the spectral properties of the Floquet system. In accordance with the solution of the interacting model at finite temperatures, we use the Wigner coordinates

$$t_{\text{ave}} = (t + t')/2, \quad t_{\text{rel}} = t - t', \quad (25)$$

to define the Fourier transform with respect to relative time as

$$\begin{aligned} G_{p,\alpha\alpha}(t_{\text{ave}}, \omega) &= \int_{-\infty}^{\infty} dt_{\text{rel}} e^{i(\omega + i\eta)t_{\text{rel}}} \\ &\times G_{p,\alpha\alpha}(t_{\text{ave}} + t_{\text{rel}}/2, t_{\text{ave}} - t_{\text{rel}}/2). \end{aligned} \quad (26)$$

For the interacting model at finite temperatures, we find that the system reaches a steady state where the local spectral functions turn out to be positive semidefinite for any t_{ave} that is large enough. For the zero-temperature case with a single phonon configuration, the system does not decay but keeps oscillating forever. It has been proved that the spectral function of the retarded Green's function is positive semidefinite if one averages t_{ave} over the Floquet period T [3]. However, in our single-particle calculation for the lesser Green's function, we need to average over time-dependent exponentials including the real-valued quasienergies $\epsilon_\nu \in [-\Omega/2, \Omega/2]$ as follows:

$$\begin{aligned} \lim_{T \rightarrow \infty} \frac{1}{T} \int_{-T/2}^{T/2} dt_{\text{ave}} e^{-i[\epsilon_\mu - \epsilon_\nu + (m - m')\Omega]t_{\text{ave}}} \\ = \lim_{T \rightarrow \infty} \text{sinc}\{[\epsilon_\mu - \epsilon_\nu + (m - m')\Omega]T/2\} \\ = \delta_{\mu\nu} \delta_{mm'}. \end{aligned} \quad (27)$$

Because $\text{sinc}(0) = 1$, $\text{sinc}(\pm\infty) = 0$, and assuming that the ϵ_ν are nondegenerate, we obtain the Kronecker delta. Hence, we define the spectral functions as follows:

$$\bar{A}_{p\alpha}(\omega) = -\lim_{T \rightarrow \infty} \frac{1}{\pi T} \int_{-T/2}^{T/2} dt_{\text{ave}} \text{Im} G_{p,\alpha\alpha}^{\text{ret}}(t_{\text{ave}}, \omega), \quad (28)$$

$$\bar{A}_{p\alpha}^<(\omega) = \lim_{T \rightarrow \infty} \frac{1}{2\pi T} \int_{-T/2}^{T/2} dt_{\text{ave}} \text{Im} G_{p,\alpha\alpha}^<(t_{\text{ave}}, \omega). \quad (29)$$

This definition assumes that the initial time when the field is turned on fulfills $t_0 \rightarrow -\infty$. As discussed in more detail below, these definitions correspond to the steady-state spectra at $k_B T \rightarrow 0$.

In the following, we derive analytic expressions for the spectral functions. Because we are using the temporal gauge, the p resolved spectral functions will be gauge dependent. We are mainly interested in the local spectra which are summed over all p and therefore become gauge invariant again. To calculate momentum dependent observables, we have to substitute $p \rightarrow p - Et_{\text{ave}}$ in the corresponding Green's functions before we perform the time average [4]. We will discuss the necessary changes further below.

1. Retarded Green's function

We first calculate the retarded Green's function. Plugging Eqs. (20) and (21) into Eq. (23), we obtain

$$G_{p,\alpha\beta}^{\text{ret}}(t, t') = -i\Theta(t - t') \sum_{\mu\nu} e^{-i\epsilon_\mu(t-t_0)} e^{i\epsilon_\nu(t'-t_0)} \times \langle p\alpha | \Phi_{p\mu}(t) \rangle \langle \Phi_{p\nu}(t') | p\beta \rangle \langle \{ \hat{c}_{p\mu}(t_0), \hat{c}_{p\nu}^\dagger(t_0) \} \rangle. \quad (30)$$

Because $\{ \hat{c}_{p\mu}(t_0), \hat{c}_{p\nu}^\dagger(t_0) \} = \delta_{\mu\nu}$, we find

$$G_{p,\alpha\beta}^{\text{ret}}(t, t') = -i\Theta(t - t') \sum_\mu e^{-i\epsilon_\mu(t-t')} \times \langle p\alpha | \Phi_{p\mu}(t) \rangle \langle \Phi_{p\mu}(t') | p\beta \rangle. \quad (31)$$

Using the time evolution of the Floquet states, we have

$$G_{p,\alpha\beta}^{\text{ret}}(t, t') = -i\Theta(t - t') \sum_\mu \sum_{mm'} e^{-i\epsilon_\mu(t-t')} e^{-im\Omega t} \times e^{im'\Omega t'} \langle p\alpha | \phi_{p\mu}^{(m)} \rangle \langle \phi_{p\mu}^{(m')} | p\beta \rangle. \quad (32)$$

If we switch to the Wigner coordinates of Eq. (25), the time-dependent exponentials become

$$e^{-i[\epsilon_\mu + (m+m')\Omega/2]t_{\text{rel}}} e^{-i(m-m')\Omega t_{\text{ave}}}. \quad (33)$$

We can now do the Fourier transform in relative time and obtain

$$G_{p,\alpha\beta}^{\text{ret}}(t_{\text{ave}}, \omega) = -\sum_\mu \sum_{mm'} \frac{\langle p\alpha | \phi_{p\mu}^{(m)} \rangle \langle \phi_{p\mu}^{(m')} | p\beta \rangle}{\epsilon_\mu + (m+m')\Omega/2 - \omega - i\eta} \times e^{-i(m-m')\Omega t_{\text{ave}}}. \quad (34)$$

Here, we explicitly see that we have to average over a period T to obtain a positive spectral function

$$\bar{A}_{p\alpha}(\omega) = \sum_\mu \sum_m |\langle p\alpha | \phi_{p\mu}^{(m)} \rangle|^2 \delta(\epsilon_\mu + m\Omega - \omega). \quad (35)$$

To show that the local spectral function is positive, we do not need to average over t_{ave} . We can just sum over p and α in Eq. (32) and use the symmetries in Eqs. (12) and (14) to obtain

$$\begin{aligned} & \frac{1}{L} \sum_{p \in [0, \pi]} \sum_\alpha \langle p\alpha | \phi_{p\mu}^{(m)} \rangle \langle \phi_{p\mu}^{(m')} | p\alpha \rangle \\ &= \frac{1}{L} \sum_{p \in [0, \pi]} e^{-ip(m-m')} (1 + e^{-i\pi(m-m')}) \\ & \quad \times \langle p = 0, \alpha = 1 | \phi_{p=0,\mu}^{(m)} \rangle \langle \phi_{p=0,\mu}^{(m')} | p = 0, \alpha = 1 \rangle \\ &= \frac{1}{L} \sum_{p \in [0, 2\pi]} e^{-ip(m-m')} \\ & \quad \times \langle p = 0, \alpha = 1 | \phi_{p=0,\mu}^{(m)} \rangle \langle \phi_{p=0,\mu}^{(m')} | p = 0, \alpha = 1 \rangle \\ &= \delta_{mm'} |\langle p = 0, \alpha = 1 | \phi_{p=0,\mu}^{(m)} \rangle|^2. \end{aligned} \quad (36)$$

Here, the average over p has the same effect as the average over a period T .

2. Lesser Green's function

In the same way, we find that the lesser Green's function satisfies

$$-iG_{p,\alpha\beta}^<(t, t') = \sum_{\mu\nu} e^{-i\epsilon_\mu(t-t_0)} e^{i\epsilon_\nu(t'-t_0)} \times \langle p\alpha | \Phi_{p\mu}(t) \rangle \langle \Phi_{p\nu}(t') | p\beta \rangle \langle \hat{c}_{p\nu}^\dagger(t_0) \hat{c}_{p\mu}(t_0) \rangle. \quad (37)$$

The dependence on the equal-time expectation value at t_0 makes computations more difficult. Using the Fourier expansion of the Floquet states, we have

$$\begin{aligned} -iG_{p,\alpha\beta}^<(t, t') &= \sum_{\mu\nu} \sum_{mm'} e^{-i(\epsilon_\mu + m\Omega)t} e^{i(\epsilon_\nu + m'\Omega)t'} e^{i(\epsilon_\mu - \epsilon_\nu)t_0} \\ & \quad \times \langle p\alpha | \phi_{p\mu}^{(m)} \rangle \langle \phi_{p\nu}^{(m')} | p\beta \rangle \langle \hat{c}_{p\nu}^\dagger(t_0) \hat{c}_{p\mu}(t_0) \rangle. \end{aligned} \quad (38)$$

If we switch to Wigner coordinates, the time-dependent exponentials become

$$e^{-i[\epsilon_\mu - \epsilon_\nu + (m-m')\Omega]t_{\text{ave}}} e^{-i[\epsilon_\mu + \epsilon_\nu + (m+m')\Omega]t_{\text{rel}}/2} e^{i(\epsilon_\mu - \epsilon_\nu)t_0}. \quad (39)$$

As discussed above, we have to average t_{ave} over all times to obtain a positive weight. We find that

$$\begin{aligned} -i\bar{G}_{p,\alpha\beta}^<(\omega) &= 2\pi \sum_\mu \sum_m \langle p\alpha | \phi_{p\mu}^{(m)} \rangle \langle \phi_{p\mu}^{(m)} | p\beta \rangle \\ & \quad \times \langle \hat{c}_{p\mu}^\dagger(t_0) \hat{c}_{p\mu}(t_0) \rangle \delta(\epsilon_\mu + m\Omega - \omega). \end{aligned} \quad (40)$$

From this, we can see that the momentum resolved spectrum $\bar{A}_{p\alpha}^<(\omega)$ (and therefore also the local spectrum) is always positive semidefinite, i.e.,

$$\begin{aligned} \bar{A}_{p\alpha}^<(\omega) &= \sum_{\mu m} \left\| \hat{c}_{p\mu}(t_0) |GS\rangle \right\|^2 \left| \langle p\alpha | \phi_{p\mu}^{(m)} \rangle \right|^2 \\ &\times \delta(\epsilon_\mu + m\Omega - \omega). \end{aligned} \quad (41)$$

For simplicity of notation, we assumed that the expectation value is with respect to the ground state $|GS\rangle$.

In contrast to the retarded Green's function, there is no obvious way to show that the spectrum of the local lesser Green's function is positive without also performing a time average. The nontrivial momentum dependence of the initial state makes this calculation much more difficult. After performing the time average, it becomes positive semidefinite as it must, since it is just a sum over all momenta of the positive semidefinite $\bar{A}_{p\alpha}^<(\omega)$.

3. Distribution function

We can now calculate the nonequilibrium distribution function as the ratio of lesser and retarded spectral functions, i.e.,

$$\bar{f}_{\infty,p\alpha}(\omega) = \frac{\bar{A}_{p\alpha}^<(\omega)}{\bar{A}_{p\alpha}(\omega)}. \quad (42)$$

For our noninteracting model at $k_B T = 0$ we find

$$\bar{f}_{\infty,p\alpha}(\epsilon_\mu + m\Omega) = \langle \hat{c}_{p\mu}^\dagger(t_0) \hat{c}_{p\mu}(t_0) \rangle. \quad (43)$$

Interestingly, the distribution function averaged over all time corresponds to the average occupation of a Floquet state at the initial time. Therefore, the distribution function for a Floquet level is determined by the overlap of the corresponding Floquet state with the initial state. However, this p resolved ratio is not gauge invariant. To this end, we calculate the ratio of the local spectral functions and see that

$$\bar{f}_\infty(\epsilon_\mu + m\Omega) = \frac{2}{L} \sum_{p \in [0, \pi)} \langle \hat{c}_{p\mu}^\dagger(t_0) \hat{c}_{p\mu}(t_0) \rangle. \quad (44)$$

Here, we used Eq. (12) to show that $|\langle p\alpha | \phi_{p\mu}^{(m)} \rangle|^2$ is independent of p and therefore drops out of the ratio. Remarkably, the local ratio \bar{f}_∞ fully determines the gauge-invariant steady-state observables, even the momentum-dependent ones. This will become clear below.

E. Steady-state observables

Although the time-dependent observables at zero temperature do not decay towards a steady state, we can define the time average

$$\langle \hat{O} \rangle_\infty = \lim_{T \rightarrow \infty} \frac{1}{T} \int_{t_0}^{t_0+T} dt \langle \hat{O}(t) \rangle, \quad (45)$$

which is consistent with the steady-state value in the interacting model. Here, t_0 is the time when the field is turned on. We will see below that this definition reproduces compatible results.

1. Gauge-invariant momentum distribution function

We want to calculate the momentum-distribution function in the steady state. For this, we have to consider the gauge-invariant form [4]

$$n(k, t) = -i G_{p-Et, \alpha\alpha}^<(t, t) \quad (46)$$

where $k = p + (\alpha - 1)\pi$. Starting from the lesser Green's function defined in Eq. (37), we have to properly incorporate the time-dependent momentum shifts. First, we simplify the matrix elements $\langle p - Et, \alpha | \Phi_{p-Et, \mu}(t) \rangle$ using the Fourier expansion in Eq. (3) with $\Omega = E$ and then using the momentum translation symmetry in Eq. (12). We find that

$$\begin{aligned} \langle p - Et, \alpha | \Phi_{p-Et, \mu}(t) \rangle &= \sum_m e^{-im\Omega t} \langle p - Et, \alpha | \phi_{p-Et, \mu}^{(m)} \rangle \\ &= \sum_m e^{-im\Omega t} e^{-im(p-Et)} \langle p = 0, \alpha | \phi_{p=0, \mu}^{(m)} \rangle \\ &= \langle p\alpha | \Phi_{p\mu}(t=0) \rangle, \end{aligned} \quad (47)$$

where the time dependence has dropped out due to the gauge transformation. Second, we observe that the expectation value $\langle \hat{c}_{p-Et, \nu}^\dagger(t_0) \hat{c}_{p-Et, \mu}(t_0) \rangle$ is a periodic function in time with period $T = 2\pi/E$, so that it can be expanded in a Fourier series. Its time dependence is given by $e^{-im\Omega t}$ and together with the factor $e^{-i(\epsilon_\mu - \epsilon_\nu)t}$ from Eq. (37), the time average in Eq. (45) leads to $\delta_{\mu\nu} \delta_{\tilde{m}0}$. The zeroth element of the expectation value is given by

$$\begin{aligned} \frac{1}{T} \int_0^T dt \langle \hat{c}_{p-Et, \mu}^\dagger(t_0) \hat{c}_{p-Et, \mu}(t_0) \rangle \\ \cong \frac{2}{L} \sum_p \langle \hat{c}_{p\mu}^\dagger(t_0) \hat{c}_{p\mu}(t_0) \rangle = \bar{f}_\infty(\epsilon_\mu). \end{aligned} \quad (48)$$

Because in the thermodynamic limit the time average over a period is equivalent to an average over all momenta, the expectation value reduces to the local distribution function $\bar{f}_\infty(\epsilon_\mu)$. With this, the gauge-invariant momentum distribution function becomes

$$\bar{n}_\infty(k) = \sum_\mu |\langle p\alpha | \Phi_{p\mu}(t=0) \rangle|^2 \bar{f}_\infty(\epsilon_\mu). \quad (49)$$

In particular, if $\bar{f}_\infty(\epsilon_\mu) = 1/2$ for both Floquet levels μ , we can use the completeness of the Floquet states to show that $\bar{n}_\infty(k) = 1/2$ for all k , as we would expect for an infinite-temperature state.

2. Total energy

To determine the total energy of the steady state, we do not need to use the gauge-invariant Green's function

because we sum over all p . Again, we can easily calculate the average over time using Floquet theory. For single-particle observables at equal times, we expand

$$\hat{O}(t) = \sum_p \sum_{\alpha\beta} O_{p,\alpha\beta}(t) [-i G_{p,\beta\alpha}^<(t,t)]. \quad (50)$$

We can directly calculate the electron-phonon energy, because its matrix element has no time dependence. We have that

$$E_{\text{eph}}^{\infty} = \Delta \sum_{p\alpha} \sum_{\mu m} \langle p\alpha | \phi_{p\mu}^{(m)} \rangle \langle \phi_{p\mu}^{(m)} | p\bar{\alpha} \rangle \langle \hat{c}_{p\mu}^{\dagger}(t_0) \hat{c}_{p\mu}(t_0) \rangle. \quad (51)$$

For the kinetic energy, we must include the time dependence of the electric field. Therefore, we use the Fourier series of the matrix element to obtain

$$E_{\text{kin}}^{\infty} = \sum_{p\alpha} \sum_{s=\pm 1} \mathcal{H}_{p,\alpha\alpha}^{(s)} \sum_{\mu m} \langle p\alpha | \phi_{p\mu}^{(m)} \rangle \times \langle \phi_{p\mu}^{(m+s)} | p\alpha \rangle \langle \hat{c}_{p\mu}^{\dagger}(t_0) \hat{c}_{p\mu}(t_0) \rangle. \quad (52)$$

A better understanding of the steady-state energies can be obtained by starting from the gauge-invariant form. If we substitute $p \rightarrow p - Et$ in Eq. (50), we find that $\mathcal{H}_{p-Et,\alpha\beta}(t) = \mathcal{H}_{p,\alpha\beta}(t=0)$ loses its time dependence. Therefore, the time average only applies to the lesser Green's function. As before we can derive

$$-i G_{p-Et,\beta\alpha}^<(t,t) = \sum_{\mu} \langle p\beta | \Phi_{p\mu}(t=0) \rangle \times \langle \Phi_{p\mu}(t=0) | p\alpha \rangle \bar{f}_{\infty}(\epsilon_{\mu}). \quad (53)$$

If $\bar{f}_{\infty}(\epsilon_{\mu}) = 1/2$ for both Floquet levels, we can use the completeness of the Floquet states to obtain the matrix element $\langle p\beta | p\alpha \rangle = \delta_{\alpha\beta}$. Then, we find that $E_{\text{eph}}^{\infty} = 0$ because $\mathcal{H}_{p,\alpha\beta}(t=0)$ has only off-diagonal entries. We also find that $E_{\text{kin}}^{\infty} = 0$ because the diagonal elements cancel each other. Again, these results are consistent with an infinite-temperature state.

3. Gauge-invariant spectral functions

Finally, we want to discuss how the spectral functions change if we start from the gauge-invariant Green's functions. For the retarded Green's function, the substitution $p \rightarrow \bar{p} = p - Et_{\text{ave}}$ will only eliminate the factor $e^{-i(m-m')\Omega t_{\text{ave}}}$ in Eq. (34) and we obtain

$$\bar{A}_{\bar{p}\alpha}(\omega) = \sum_{\mu} \sum_{mm'} \langle p\alpha | \phi_{p\mu}^{(m)} \rangle \langle \phi_{p\mu}^{(m')} | p\alpha \rangle \times \delta[\epsilon_{\mu} + (m+m')\Omega/2 - \omega]. \quad (54)$$

For the lesser Green's function, we have to average over t_{ave} to obtain

$$\bar{A}_{\bar{p}\alpha}^<(\omega) = 2\pi \sum_{\mu} \bar{f}_{\infty}(\epsilon_{\mu}) \sum_{mm'} \langle p\alpha | \phi_{p\mu}^{(m)} \rangle \langle \phi_{p\mu}^{(m')} | p\alpha \rangle \times \delta[\epsilon_{\mu} + (m+m')\Omega/2 - \omega]. \quad (55)$$

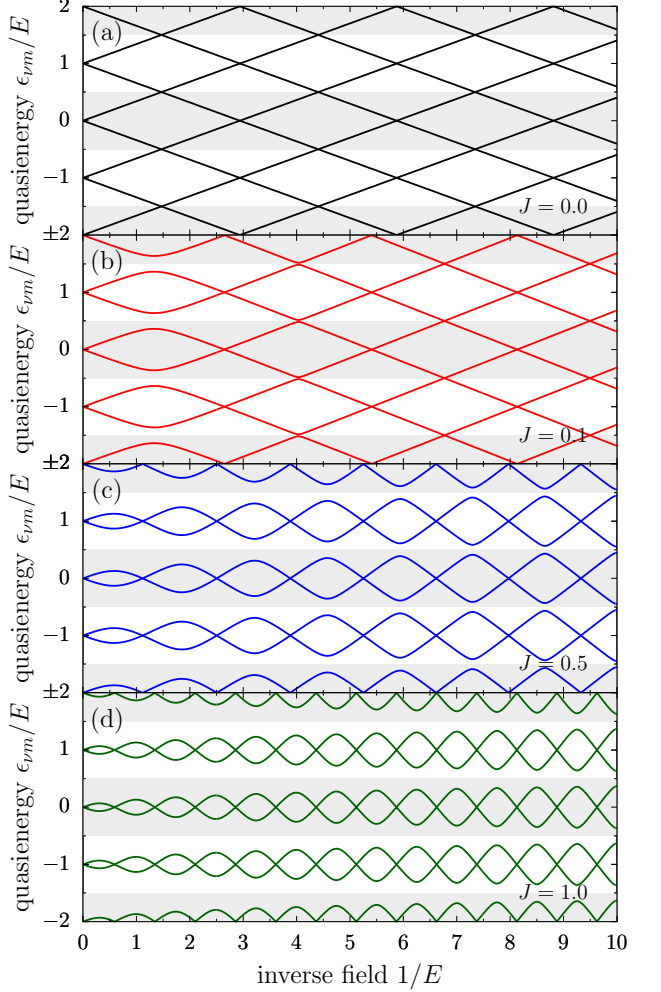


FIG. 1. Floquet quasienergies for $\Delta = 0.3404$ as a function of inverse electric field for (a) $J = 0.0$, (b) $J = 0.1$, (c) $J = 0.5$, and (d) $J = 1.0$. The hopping amplitude J leads to avoided level crossings at the Floquet zone boundaries.

In the gauge-invariant form, the ratio of the momentum-resolved spectral functions is just given by the local ratio $\bar{f}_{\infty}(\epsilon_{\mu})$. Although we cannot prove positive-definiteness for either of the spectra, their ratio is given by a positive function. To obtain positive spectral functions, we still have to sum over all momenta as in Eq. (36) in order to reproduce our previous results.

II. ADDITIONAL RESULTS

A. Zero temperature

As we have seen in the previous section, the Holstein model can be solved efficiently at zero temperature using Floquet theory. Although the system never reaches a steady state with zero current and constant energy at $k_B T = 0$ (as occurs for all $k_B T > 0$), we still obtain impor-

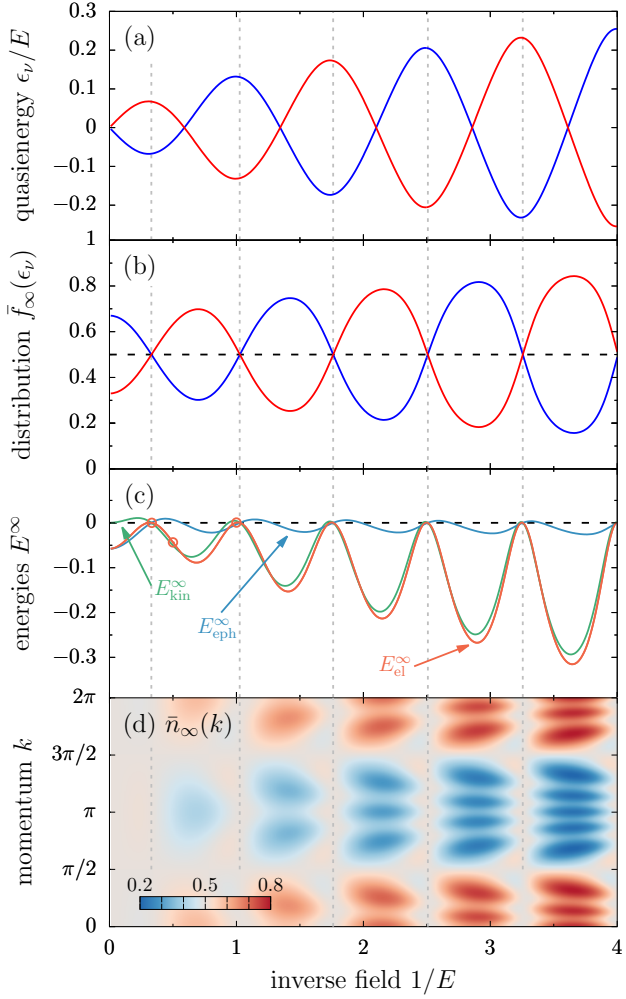


FIG. 2. Solution of the Holstein model at $k_B T = 0$ as a function of inverse electric field. (a) Floquet quasienergies within the first Floquet zone and (b) the corresponding distribution function $\bar{f}_\infty(\epsilon_\nu)$. (c) Time-averaged energies. (d) Gauge-invariant momentum distribution function. The black dashed lines in (b) and (c) correspond to the infinite-temperature solution. Vertical lines mark the electric-field values where avoided level crossings occur. Open circles in (c) correspond to the exact ground-state energies of the fields considered in Fig. 5. Here, $\Delta = 0.3404$ and $J = 1$.

tant insights from the $k_B T = 0$ solution into the nature of the steady state and the heating process at $k_B T > 0$. In the following, we expand on our discussion of the $k_B T = 0$ case presented in the main article.

The Floquet energy spectrum of our two-band model consists of two interpenetrating Wannier-Stark ladders. Figure 1 illustrates the gap opening at the Floquet zone boundaries for different hopping amplitudes J and fixed $\Delta = 0.3404$. For $J \rightarrow 0$, the two ladders are independent of each other and the exact energies are $\epsilon_{\nu m} = \pm\Delta + mE$. The corresponding energy spectrum in Fig. 1(a) shows level crossings both at the Floquet zone boundary and center. With increasing J , the spectrum opens up a gap

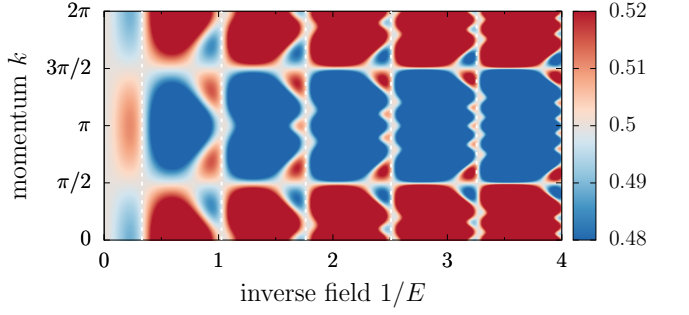


FIG. 3. Close-up of the gauge-invariant momentum distribution function shown in Fig. 2(d). For better visibility of the delocalization features, we restrict the color range to $\bar{n}_\infty(k) \in [0.48, 0.52]$. Vertical lines mark the electric-field values where avoided level crossings occur. Here, $\Delta = 0.3404$ and $J = 1$.

at the Floquet zone boundary that is largest for strong fields, as shown in Figs. 1(b)–(d). Moreover, the avoided level crossings shift towards stronger fields with increasing J . On the other side, the level crossings at the Floquet zone center remain.

In Fig. 2, we compare the occurrence of level crossings and avoided crossings in the energy spectrum to the system's ability to distribute the energy absorbed from the electric field. Figure 2(a) shows the two quasienergy levels ϵ_ν in the first Floquet zone as a function of $1/E$. The corresponding distribution functions $\bar{f}_\infty(\epsilon_\nu)$ in Fig. 2(b) give the time-averaged probability of finding an electron in one of the levels. At a set of exceptional points we find $\bar{f}_\infty(\epsilon_\nu) = 1/2$ for both levels, which is the analog to an infinite-temperature state. Away from these points, either the lower or the upper Floquet level has a higher occupation which corresponds to an effective positive or negative temperature. Moreover, the time-averaged electronic energy in Fig. 2(c) reaches its infinite-temperature limit $E_{\text{el}} = 0$ at these avoided level crossings. Furthermore, at these resonances, the system efficiently redistributes the energy absorbed from the electric field. In contrast, near the level crossings at the Floquet zone center, the average energy is much lower. We will demonstrate below that the time-averaged energies of the non-decaying system at $k_B T = 0$ correctly predicts the $k_B T \rightarrow 0$ limit of the true steady state at finite initial temperatures. Finally, the gauge-invariant momentum distribution function $\bar{n}_\infty(k)$ in Fig. 2(d) becomes completely flat when $\bar{f}_\infty(\epsilon_\mu) = 1/2$, as proved above. Away from the avoided level crossings, $\bar{n}_\infty(k)$ increasingly gains more features with each resonance that is crossed. A similar structure had been observed for the time-dependent oscillations of the density matrix [5]. From Fig. 2(d), it seems that $\bar{n}_\infty(k) < 1/2$ for all $\pi/2 < k < 3\pi/2$, as in the initial state. For better visibility of the detailed structure near $\bar{n}_\infty(k) = 1/2$, we show the same data again in Fig. 3 but for a smaller range of $\bar{n}_\infty(k)$. Close to the resonances, we also find regimes where the sign structure

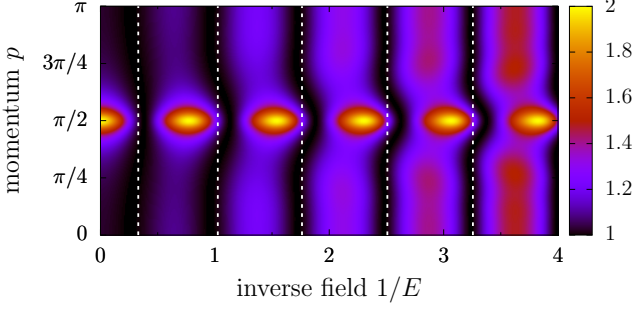


FIG. 4. Inverse participation ratio, as defined in Eq. (56), as a function of inverse field and momentum. Vertical lines mark the electric-field values where avoided level crossings occur. Here, $\Delta = 0.3404$ and $J = 1$.

of $\bar{n}_\infty(k)$ is reversed.

The avoided level crossings of the field-driven two-band model have been associated with resonance-induced delocalization in coupled Wannier-Stark ladders, both theoretically [6] and experimentally [7]. We can gain further insight into the localization properties of our Floquet system from the inverse participation ratio. We define

$$\text{IPR}(p) = \sum_{s\mu} |\langle ps|\Phi_{p\mu}(t=0)\rangle|^4 \quad (56)$$

from the overlap of the Floquet states at $t = 0$ with the energy eigenstates $|ps\rangle$ of the system at equilibrium. We have $\text{IPR}(p) = 2$ if the Floquet states are perfectly localized in the energy eigenbasis, i.e., they coincide with one of the two equilibrium eigenstates. On the other hand, $\text{IPR}(p) = 1$ for perfectly delocalized Floquet states that are an equal superposition of the equilibrium eigenstates. Figure 4 shows $\text{IPR}(p)$ as a function of $1/E$. Indeed, the avoided level crossings appear at the field strengths where the equilibrium eigenstates transform into both Floquet states with equal weight, but the delocalization is not perfect, since the minimum of $\text{IPR}(p)$ slightly depends on p . Moreover, Wannier-Stark localization is strongest between the avoided crossings and near $p = \pi/2$, where the gap of the equilibrium system is smallest. We have seen that $\text{IPR}(p)$ gives us some insight into the delocalization properties, but one has to be careful with far-reaching conclusions. $\text{IPR}(p)$ only tells us how the initial eigenstates transform into the Floquet states at $t = 0$. While the latter govern the time evolution by a period T , they do not tell us how states are occupied at intermediate times. To obtain properly-defined steady-state averages, we need to know the occupation at all times. In addition, the issue of gauge invariance would occur again if we want to get access to the physical momentum k .

B. Finite temperatures

After having expanded on the zero-temperature solution, we also want to extend our discussion of the inter-

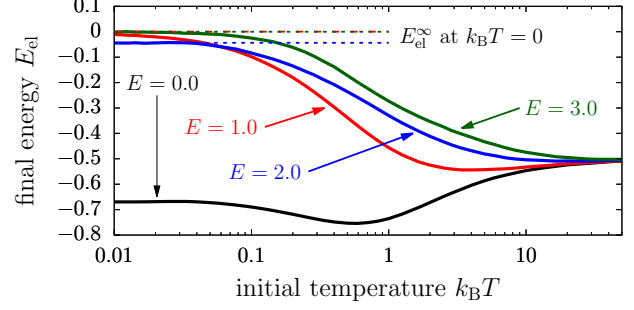


FIG. 5. Electronic energy of the steady state as a function of initial temperature for different electric fields E . The dashed lines illustrate the time-averaged energies E_{el}^∞ at $k_{\text{B}}T = 0$. Here $L = 42$, $\lambda = 0.5$.

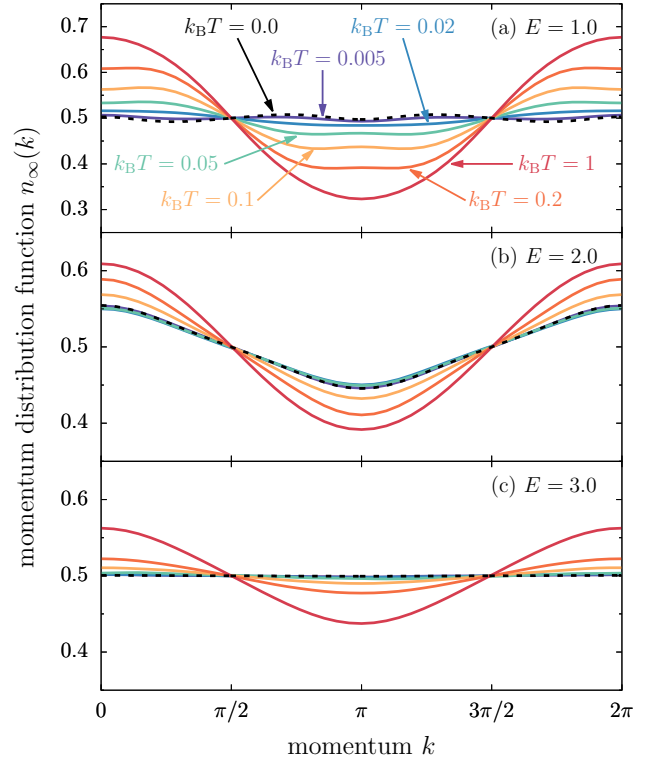


FIG. 6. Momentum distribution function of the steady state for different electric fields E and initial temperatures $k_{\text{B}}T$. Here $L = 42$, $\lambda = 0.5$.

acting system at $k_{\text{B}}T > 0$. Figure 5 shows the electronic energy of the steady state as a function of the initial temperature. We compare different electric fields to the equilibrium solution at $E = 0$. Note that the electronic energy is allowed to decrease with increasing $k_{\text{B}}T$ because the loss is compensated by an increasing phonon potential energy that is not considered here; note that static phonons cannot absorb energy from the electrons. As already discussed in our main article, the heating of the system is strongest at low initial temperatures. In particular, the time-averaged energies at $k_{\text{B}}T = 0$ —indicated

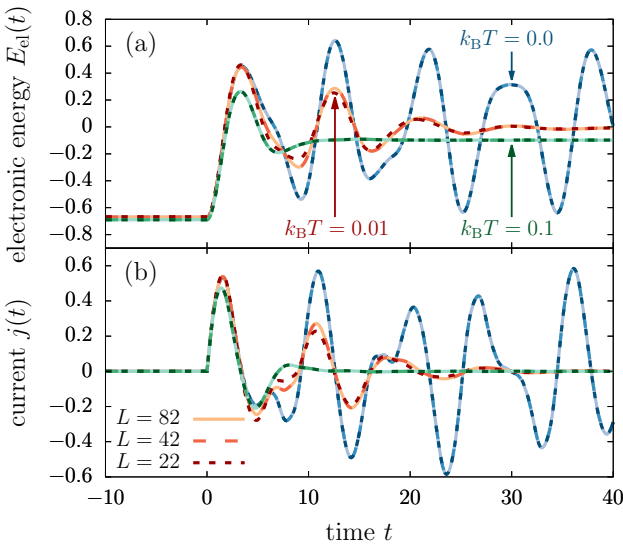


FIG. 7. Finite-size analysis of (a) the electronic energy and (b) the current for different initial temperatures. Here, $\lambda = 0.5$ and $E = 1.0$.

by the open circles in Fig. 2(c)—perfectly predict the low-temperature properties of the steady state. Therefore, the heating behavior at low $k_B T$ will show strong oscillations as a function of the electric-field strength, as shown in Fig. 2(c). In contrast, the high-temperature regime only shows weak heating effects that increase with E . This is consistent with the effect of an electric field on a strongly Anderson-localized system [8, 9]. While An-

derson localization predominantly occurs at high $k_B T$, a crossover towards Wannier-Stark localization occurs when we lower the temperature, as field effects can overcome the decreasing phonon disorder.

Figure 6 shows the momentum distribution function of the steady state for different initial temperatures and for different electric fields. Again, we confirm that the finite-temperature results approach the time-averaged Floquet solution for $k_B T \rightarrow 0$. With increasing $k_B T$, the variance of $n_\infty(k)$ increases up to $k_B T \approx 1$. This is a result of the phonon disorder which inhibits heating effects. At even higher temperatures, $n_\infty(k)$ will become flatter again, as expected for the infinite-temperature solution in equilibrium (not shown). For $E = 1$ [Fig. 6(a)] we find that the small oscillations of the $k_B T = 0$ solution survive up to $k_B T \approx 0.2$. When the field is tuned to a zero-temperature resonance [Fig. 6(c)], $n_\infty(k)$ remains almost flat up to rather high temperatures of $k_B T \approx 0.1$. These observations suggest that the Floquet physics remains relevant as long as the charge-density-wave correlations survive. In the high-temperature regime, an increasing electric field drives the system closer to an infinite-temperature state, as discussed in the main text and for the electronic energies in Fig. 5.

Finally, Fig. 7 provides a finite-size analysis of the electronic energy and the current as a function of time. We find that finite-size effects are generically small when a constant field is applied to the 1D Holstein model. Lattice sizes of $L = 42$ are sufficient for convergence within the size of the linewidth. Moreover, finite-size effects do not seem to increase with time, which allows us to evolve our system towards large average times t_{ave} .

[1] M. S. Rudner and N. H. Lindner, The Floquet Engineer’s Handbook, arXiv:2003.08252 (2020).

[2] J. H. Shirley, Solution of the Schrödinger Equation with a Hamiltonian Periodic in Time, Phys. Rev. **138**, B979 (1965).

[3] G. S. Uhrig, M. H. Kalthoff, and J. K. Freericks, Positivity of the Spectral Densities of Retarded Floquet Green Functions, Phys. Rev. Lett. **122**, 130604 (2019).

[4] R. Bertoncini and A. P. Jauho, Gauge-invariant formulation of the intracollisional field effect including collisional broadening, Phys. Rev. B **44**, 3655 (1991).

[5] J. Rotvig, A.-P. Jauho, and H. Smith, Bloch Oscillations, Zener Tunneling, and Wannier-Stark Ladders in the Time Domain, Phys. Rev. Lett. **74**, 1831 (1995).

[6] J. Leo and A. MacKinnon, Stark-Wannier states and Stark ladders in semiconductor superlattices, Journal of Physics: Condensed Matter **1**, 1449 (1989).

[7] H. Schneider, H. T. Grahn, K. v. Klitzing, and K. Ploog, Resonance-induced delocalization of electrons in GaAs-AlAs superlattices, Phys. Rev. Lett. **65**, 2720 (1990).

[8] V. N. Prigodin, One-dimensional disordered system in an electric field, JETP **52**, 1185 (1980).

[9] E. Cota, J. V. José, and G. Monsiváis, Stark-ladder resonances in ordered and disordered electrified chains, Phys. Rev. B **35**, 8929 (1987).